Supporting Information

Atomic-Scale Investigation of the Reversible α to ω-Phase Lithium Ion Charge – Discharge Characteristics of Electrodeposited Vanadium Pentoxide Nanobelts

Haytham E. M. Hussein,[†*] Richard Beanland,[‡*] Ana Sanchez,[‡] David Walker,[‡] Marc Walker,[‡] Yisong Han,[‡] and Julie V. Macpherson[†*]

[†]Department of Chemistry, University of Warwick, Coventry, CV4 7AL, UK

[‡]Department of Physics, University of Warwick, Coventry, CV4 7AL, UK

[*]Corresponding authors:

j.macpherson@warwick.ac.uk,

R.Beanland@warwick.ac.uk,

Haytham.hussein@warwick.ac.uk

Table of Contents

SI1: Experimental set-up for vanadium oxide electrodeposition and Li intercalation using the BDD-TEM electrode

A three-electrode set-up was used to electrodeposit vanadium oxide (V_2O_5) and investigate Li intercalation in aqueous media. For the electrochemical-STEM studies, the electrochemical cell is shown in Fig. S1. Note that the counter electrode is wrapped around the BDD TEM plate to provide a uniform current distribution. The BDD TEM electrode position is controlled by the micro-positioner.

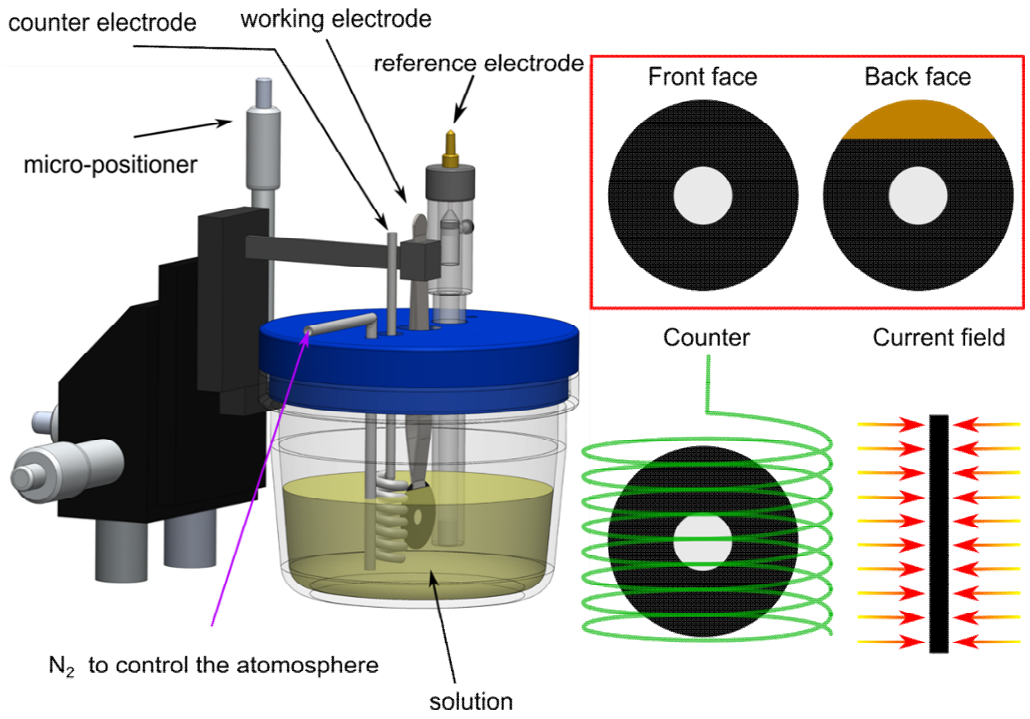

Figure S1: A schematic of the experimental cell for electrochemical deposition and lithium inter/de-intercalation experiments.

SI2: Illustration of the in-situ TEM heating set-up

To study the crystallisation behaviour of V_2O_5 in real time, the BDD-TEM electrode onto which amorphous V_2O_5 had been electrodeposited was placed into an *in-situ* heating TEM holder, Fig. S2. The holder was connected to a JEOL temperature controller.

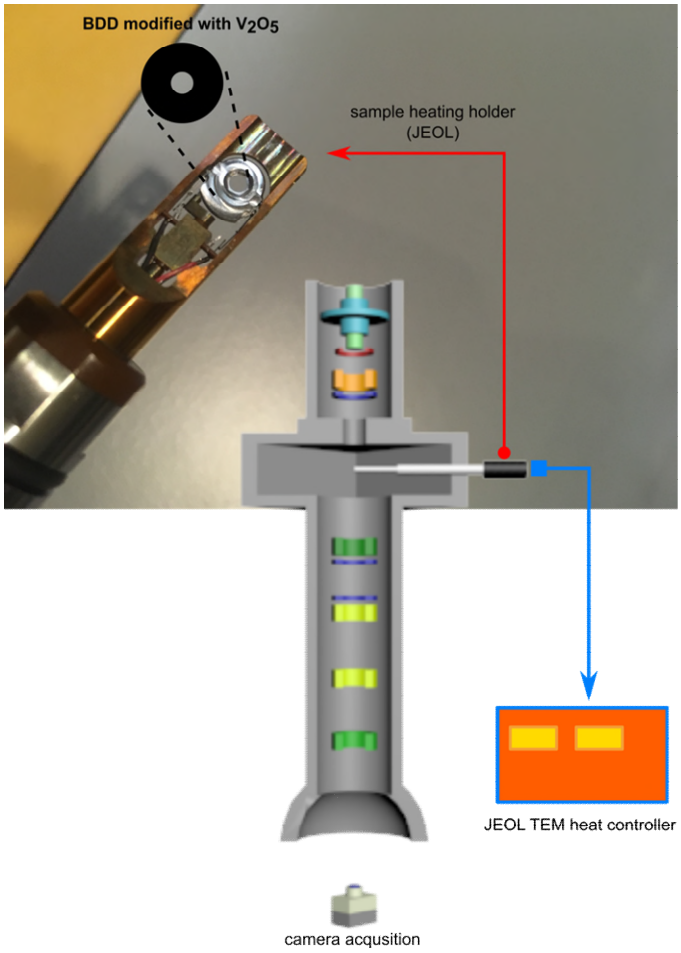

Figure S2: Image and schematic describing the *in-situ* TEM heating experiment.

SI3: Chronoamperometric response of vanadium sulphate solution using the BDD electrode in a water-DMF mixed solvent

Typical potential pulse sequence and corresponding current-time signal for the deposition of amorphous V_2O_5 on a BDD electrode

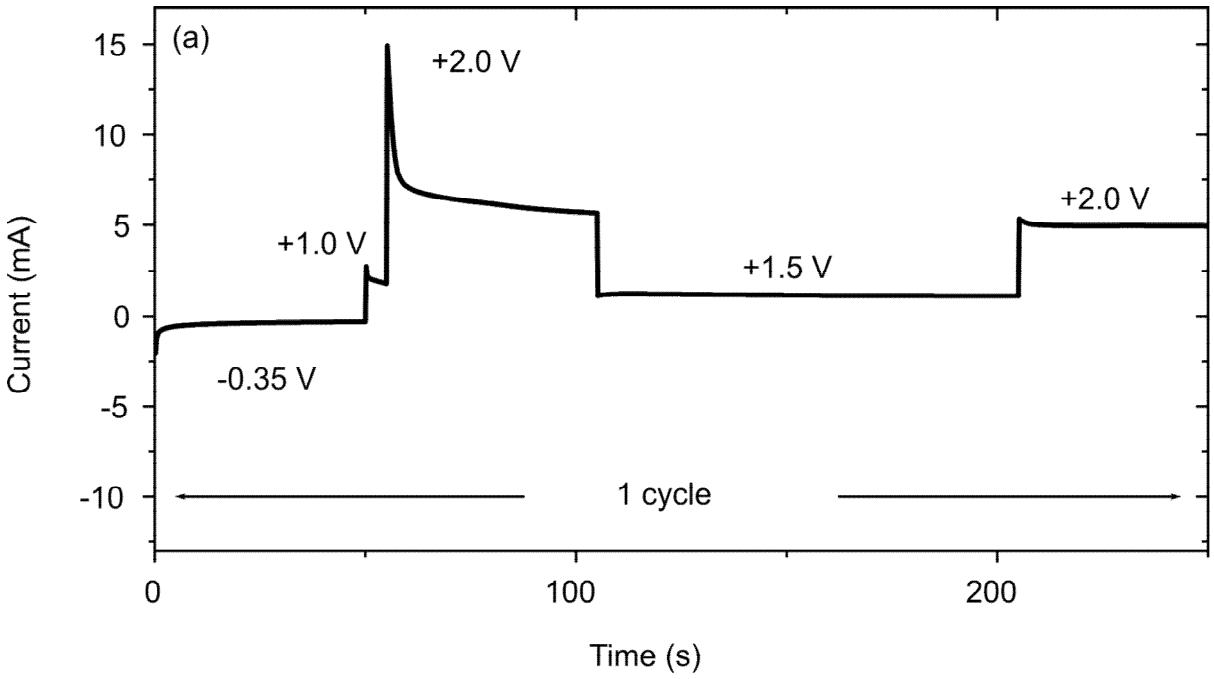

Figure S3: Chronoamperometric signal for pulsed electrodeposition of V_2O_5 on BDD

SI4: In-situ TEM thermal annealing of V_2O_5 from amorphous to crystalline

Starting from 20 °C, the BDD electrode was heated at a rate of 3.18 °C/min, and SAED snapshot images recorded of the electrodeposited V_2O_5 material (sample area ~ 2 μm^2) recorded every 15 ^oC, as shown in Fig. S4 (23 images in total).

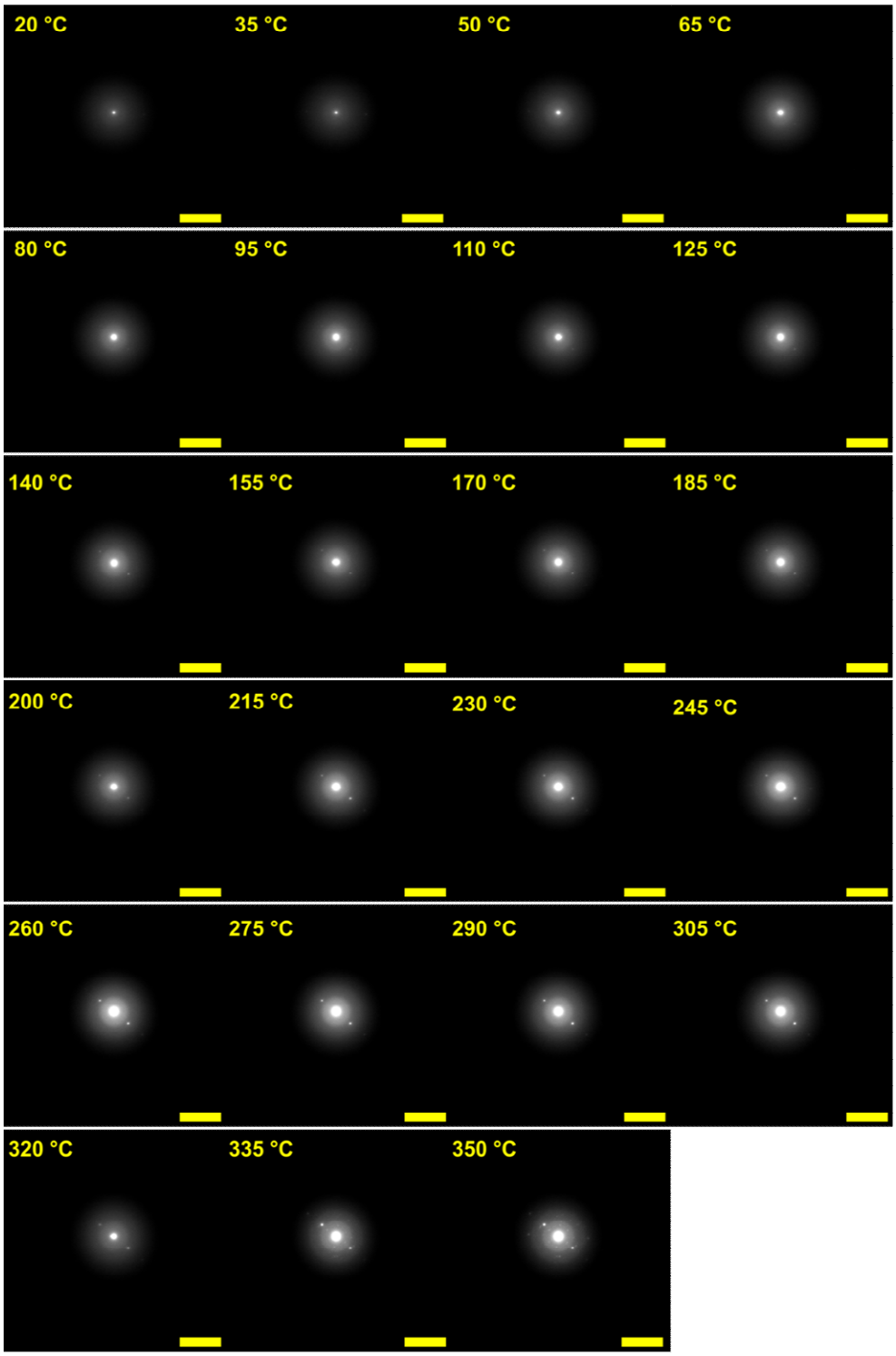

Figure S4: *In-situ* TEM heating experiment. Tracking of the transformation of the amorphous V_2O_5 electrodeposited on BDD to crystalline V_2O_5. Scale bar is 1/10 nm.

SI5: Statistical analysis of the V_2O_5 NBs dimensions and size

Statistical information on the length and width of the NBs was obtained from analysis of the ADF-STEM images. The following dimensions were determined, length = 133.35 ± 43.10 nm, and width = 9.16 ± 4.47 nm. The histogram analysis is shown in Fig. S5 and Table S1.

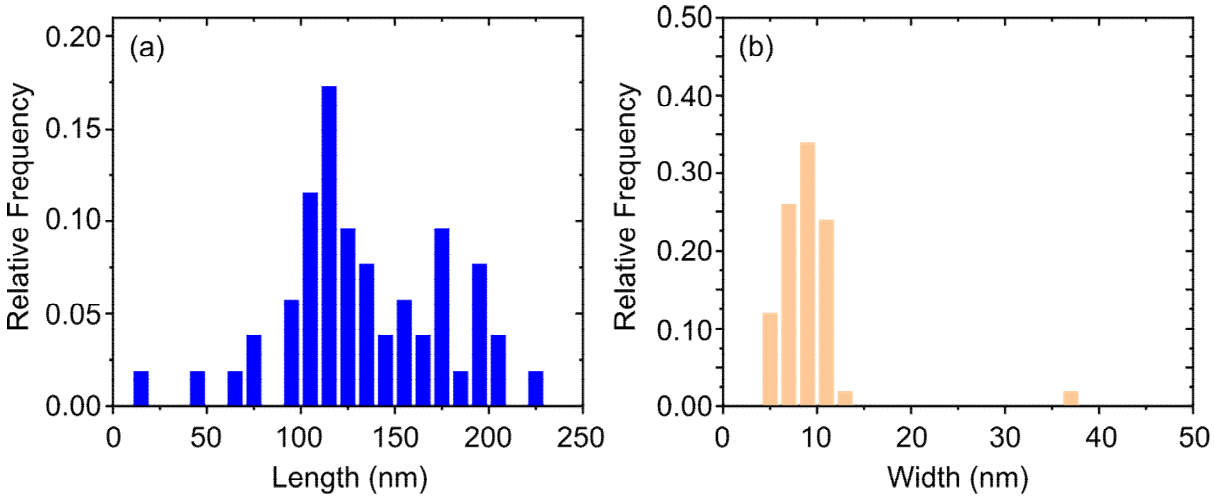

Figure S5: Histogram analysis of V_2O_5 NBs obtained using the potential pulse sequence for electrodepsotion (a) width and (b) length along the [010] growth direction, extracted from FE-SEM images and ADF-STEM images.

Table S1: Summary of analysis of the dimensions of the electrodeposited V_2O_5 NBs

	Mean	SD	Min.	**Median**	**Max.**
Length (nm)	133.35	43.1	14.74	123.2	221.4
Width (nm)	9.16	4.47	5.21	9.01	36.93

SI6: XPS survey spectrum of the crystalline V_2O_5 NBs electrodeposited on BDD

The survey spectrum indicates the material is composed of V and O as demonstrated by the XPS spectrum of the V 2p and O 1s (Fig. S6).

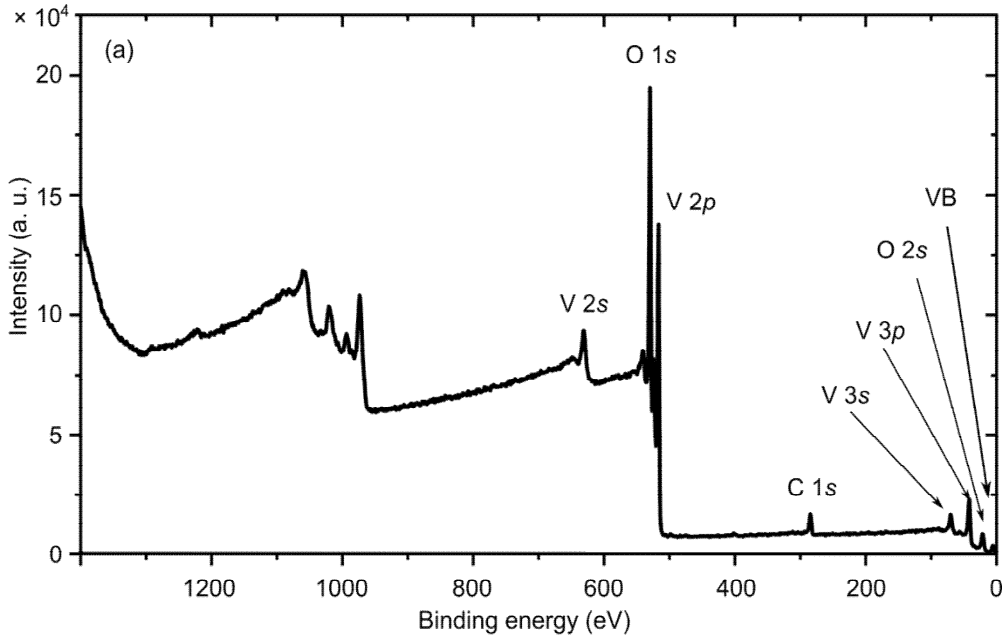

Figure S6: A survey spectrum of the crystalline V_2O_5 NBs electrodepsoited on the BDD.

SI7: Unknown vanadium oxide polymorphs

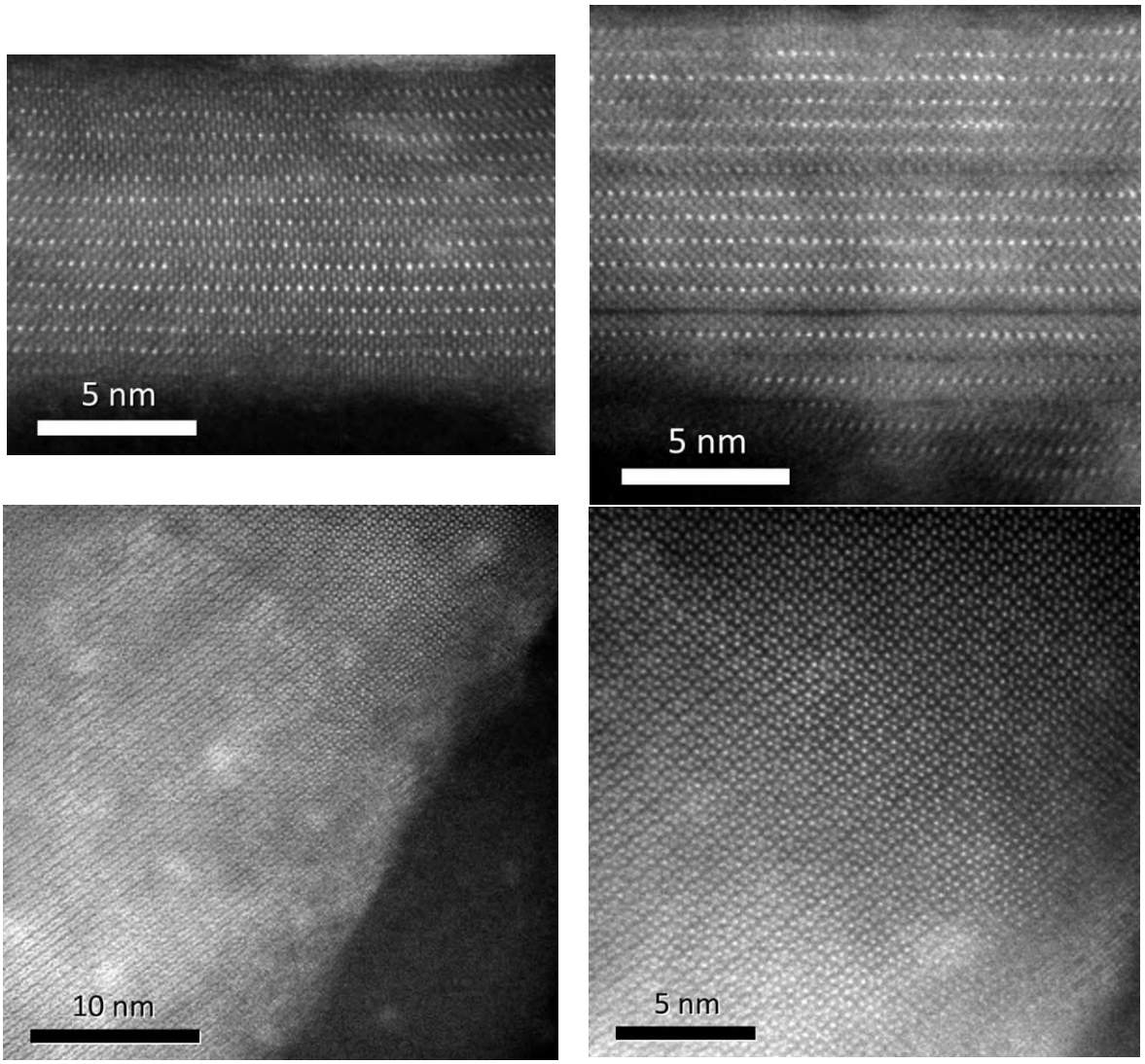

Figure S7: Occasionally, some crystals were observed by atomic resolution STEM with structures that do not correspond to any possible projection of α-V_2O_5. The upper two figures show NBs with a layered structure in which there appears to be only one fully occupied layer of vanadium (bright) and two partially occupied layers (mid-contrast). This is different to α-V_2O_5, which has two fully occupied vanadium layers and a single vacant one (*e.g.*, main text Fig. 7). The lower two figures show another unknown structure (which may simply be overlapping twin-related α-V_2O_5 crystals). Note a rocksalt (VO) altered layer is visible at the surface of this crystal.

SI8: The crystalline structure of α-V_2O_5

The structure of α-V_2O_5 and the changes that result from ion intercalation have been described in references 1 and 2. The text and data below give a brief summary of the different structures that result and provides further images of our V_2O_5 prior to lithiation studies.

Orthorhombic α-V_2O_5 is built from [VO_5] square pyramids, where one V atom lies close the square base and is surrounded by five O atoms. These square pyramids are connected by sharing the edges and corners. The crystalline structure of α-V_2O_5 along with its projected sketch from three axes is depicted in Fig. S8. The layers are held together by weak van der Waals interactions, which allows α-V_2O_5 to act as a host for ion intercalation between the layers. By imaging using ac-STEM mode, visualisation of the atomic structure of the V_2O_5 NB becomes possible using both the ADF and BF Z-contrast imaging; only atomic columns of V can be visualised in ADF contrast imaging. In ac-BF-STEM (Figs. S9a and b), the V atomic columns (orange balls) show as a dark contrast, whilst in ac-ADF-STEM, the opposite is true and. Note O atoms can be seen only in BF-STEM because the collection angle is different but this requires perfect alignment of the crystal with the e-beam. From Fig. S9a, the lattice fringes and the V atoms are visible with inter-planar spacings of d = 5.77 Å and 3.50 Å, which correspond to the (200) and the (110) set of planes, respectively. The preferential electrodeposition growth direction of the high aspect ratio V_2O_5 NBs occurs along the [100] crystal directions (a = length) (see the atomic model of V_2O_5 in Figs. S8 and S9), while the vertical (height) growth (the thickness direction or z) is less pronounced. The electrodeposition growth rate of the height (vertical thickness) is lower in comparison to the growth along horizontal axes (a = length and b = width) due to the weak V−O bond along the z direction (thickness or height). The FFT of the ac-BF-STEM image (Fig. S9b) shows a diffraction pattern of single crystalline material along the [110] axis.

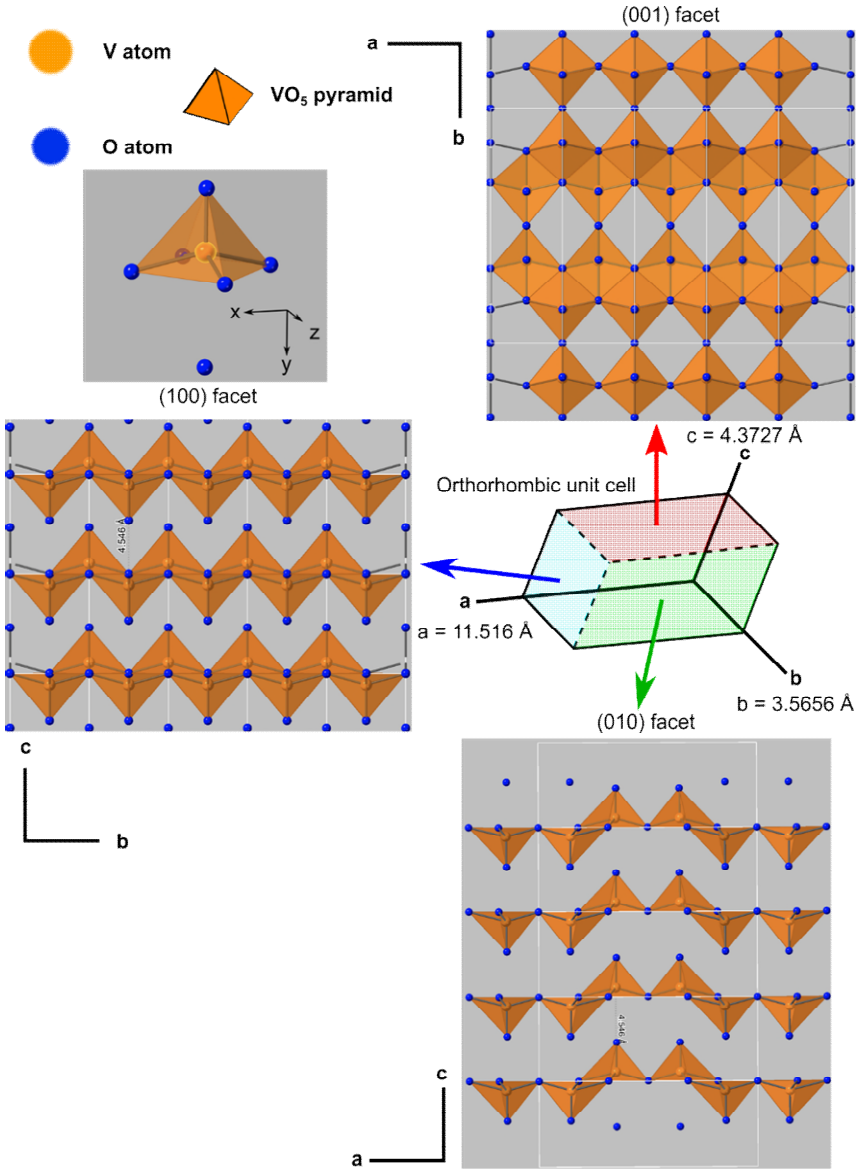

Figure S8: Demonstration of the crystalline structure of pristine α-V_2O_5 within one-unit cell. The orthorhombic unit cell of V_2O_5 is marked as white lines. Also, a crystallographic sketch with a 3D view and the projected views of (100), (010), and (001) facets are demonstrated.

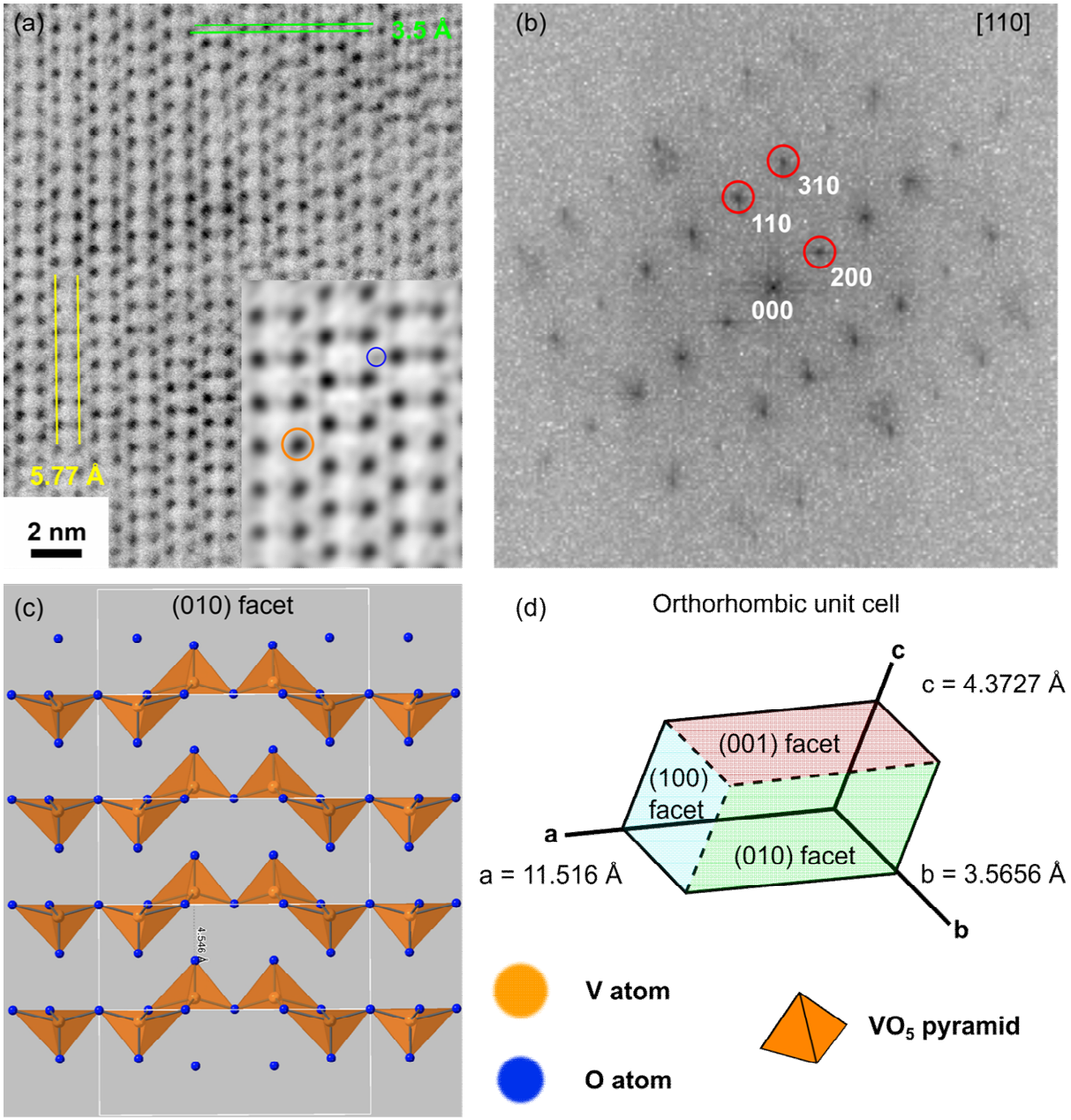

Figure S9: (a) High magnification BF-STEM image of the α-V_2O_5 NB, demonstrating the layered structure of the α-V_2O_5 and showing the atomic spacing values between the atomic columns along the (200) planes (d = 5.77 Å) and the (110) planes (d = 3.5 Å). The inset is FFT filtered image depicting the V and O atoms. (b) FFT of the α-V_2O_5 NB shown in (a), note the BF-STEM is tilted to align the V atoms vertically. (c) Atomic model from the (010) facet. (d) The orthorhombic unit cell of V_2O_5. The V atoms are presented as an orange circle, the O atoms are presented as a blue circle.

SI9: Additional observations of VO surface layers and electron dose

STEM observations of the existence of the VO layer on different NBs, Fig. S10.

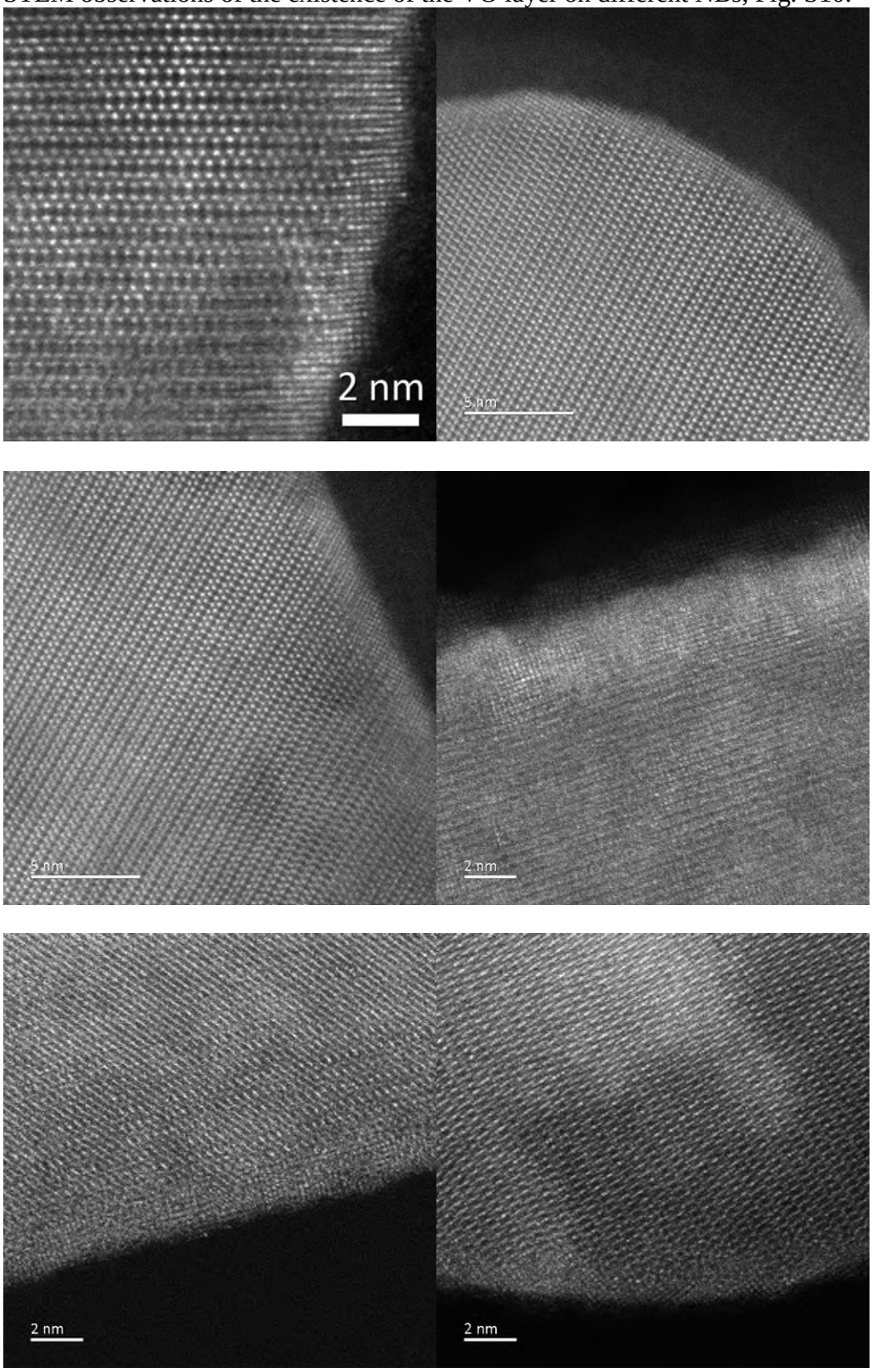

Figure S10: ADF-STEM images of V_2O_5 NBs with a VO surface layer.

A typical STEM image has a pixel size of 0.05 nm × 0.05 nm, a scan rate of 10 microseconds/pixel and a nominal probe current of 23 pA. We thus have 1.4×10^{11} electrons/second in the probe and 1.4×10^{6} electrons/pixel, giving a dose of ca. 6×10^{6} electrons/Å^2. In the work of Ai et al[3] where electron beam induced reconstruction was observed, current densities of ~2 Amps cm^{-2}, were employed, equivalent to 2×10^{-3} pA/Å^2 or 1.25×10^{7} electrons/Å^2 per second. They exposed α-V_2O_5 for periods between 5 and 100 minutes, giving doses of ~4×10^{9} to 5×10^{10} electrons/Å^2. In summary, our dose is ~1,000 time less than that used by Ai et al.[3] and thus beam damage is unlikely to be the origin of the observed VO layer.

SI10: CV data of the first discharge/charge cycle in a solution of 1 M LiCl

Lithiation and delithiation of the crystalline α-V_2O_5 NBs was also studied using CV at a scan rate of 0.05 V s^{-1} (Fig. S11) starting at 4.5 V scanning to 1.5 V and back again. This extended voltage range (*i.e.* wide potential window) was chosen rather than the more conservative range of 2.0–4.0 V as it permits intercalation of 3 Li^+ per unit cell.

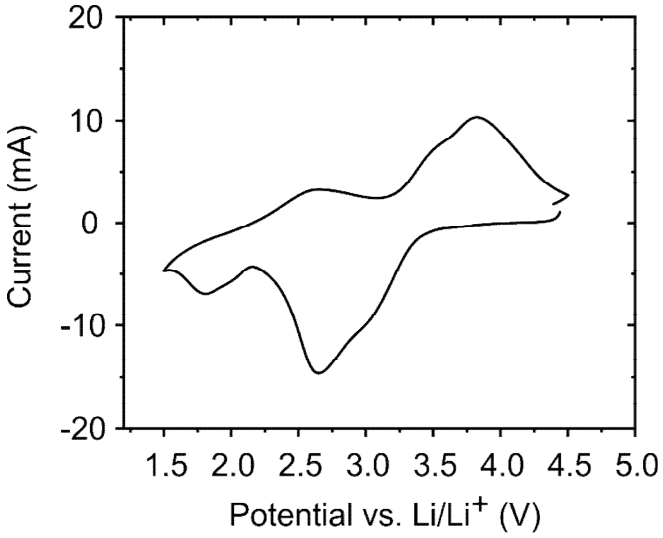

Figure S11: Electrochemical CV of the BDD electrode modified with αV_2O_5 NBs in an aqueous 1 M LiCl solution at a scan rate of 0.05 V/s.

On discharge (Li insertion / lithiation), scanning more negative from 4.5 V, the CV shows a broad peak that can be deconvoluted into two peaks at 3.05 V, and 2.80 V respectively, which are typically assigned to the phase transitions α/ε, and ε/δ respectively.[4, 5] Between 2.3 V and 1.5 V, a decrease of the current is observed, leading to another broad peak that can again be deconvoluted into two peaks. The transition to δ/γ and γ/ω phases would be expected in this region.[4, 6] By reversing the scan direction *i.e.* charging the electrode (Li extraction), two broad oxidation peaks are observed between 2.3 and 3.0 V and 3.1 V to 4.5 V, where the second peak is itself a convolution of two peaks. These three peaks are associated with Li removal from the nanostructures.

SI11: XPS and XRD of the V_2O_5 structure post Li intercalation (Li insertion)

The XPS survey spectrum of the V_2O_5 NBs after lithiation is presented in Fig. S12, which indicates the presence of V, O, and Li after the lithiation process. The Li/LiO XPS peak may indicate some NBs did not completely convert during the first cycle which left Li exposed to air during transport from the lab to the XPS instrument

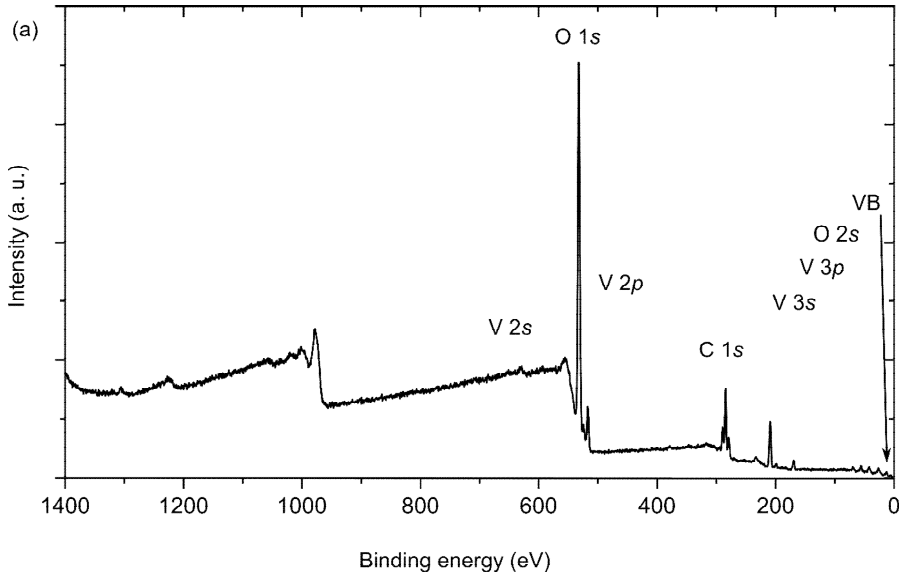

Figure S12: XPS survey spectrum of (VO)α-V_2O_5 after Li intercalation (discharge).

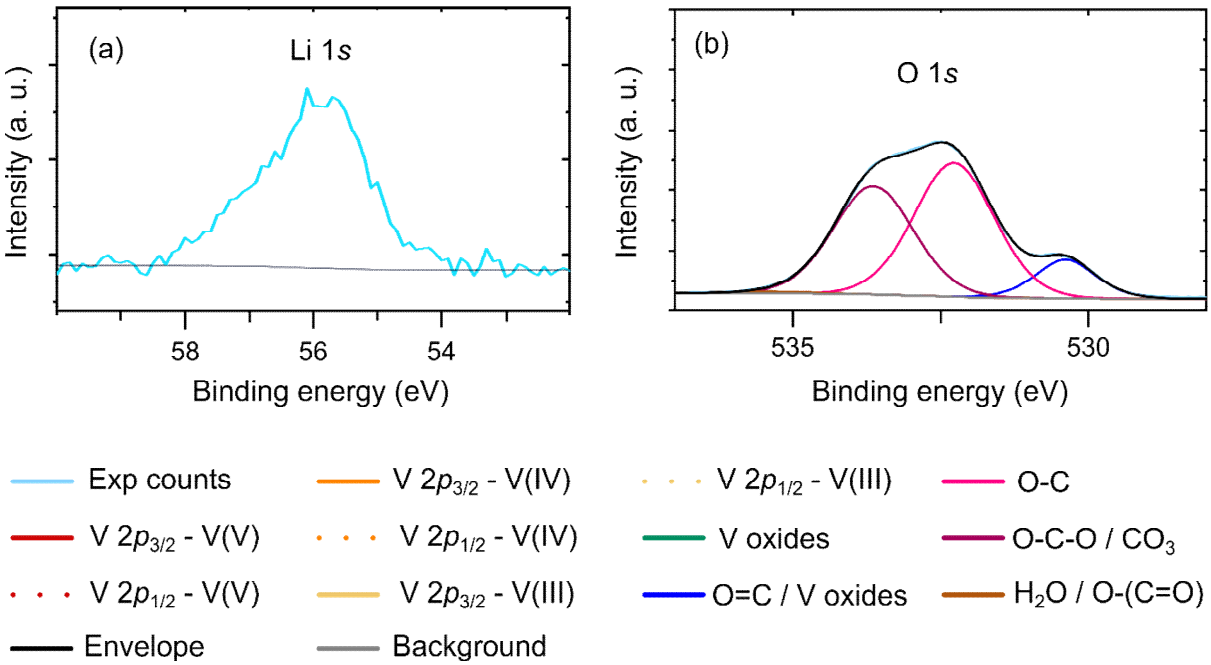

Figure S13: XPS study of the structure of the V_2O_5 NBs after lithiation (discharge). (a) XPS spectrum of the Li 1s of the $Li_3V_2O_5$ NBs after the first lithiation. (b) XPS spectrum and curve fitting of the O1s of the V_2O_5 NBs after the first lithiation.

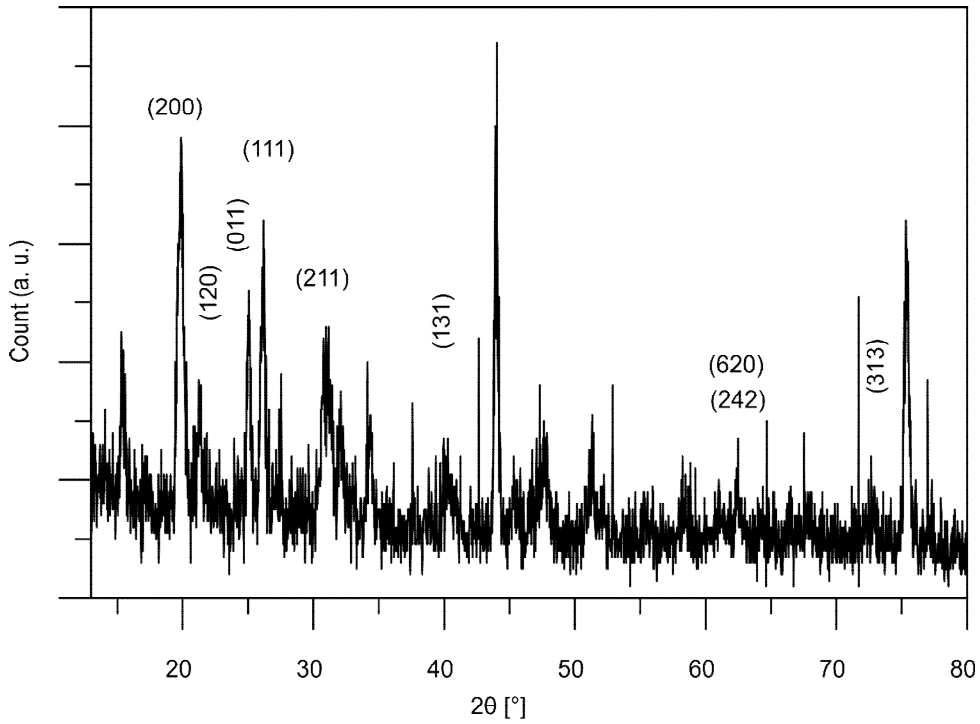

Figure S14: ω-2θ XRD pattern after the first discharge (lithiation).

SI12: XPS and XRD of the V_2O_5 structure post Li deintercalation (Li^+ removal)

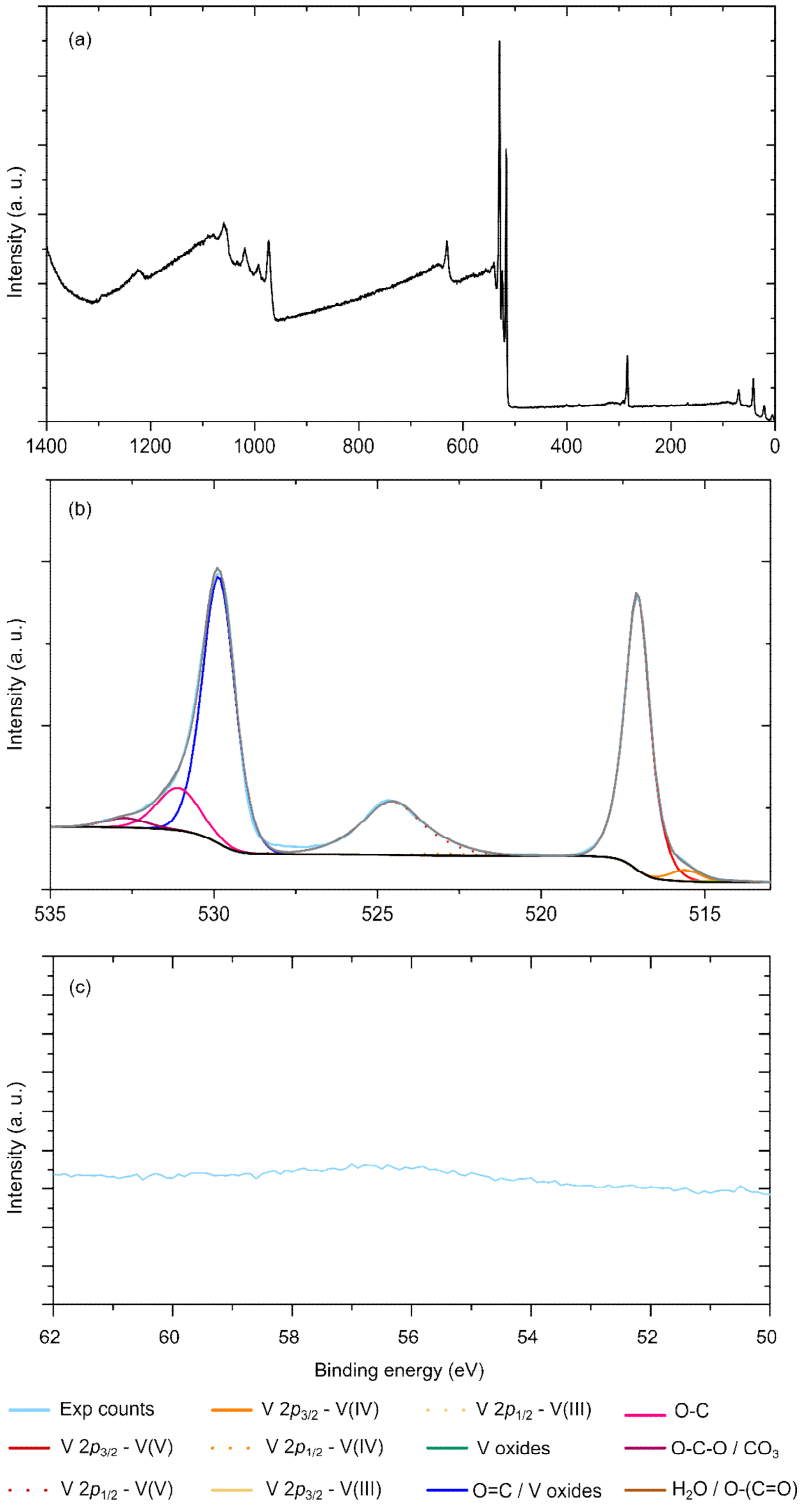

Figure S15: XPS study of the structure of the V_2O_5 NBs after delithiation (charge). (a) XPS survey spectrum of α-V_2O_5 after Li deintercalation (charge). (b) XPS spectrum and curve fitting of the V2*p* and the O1*s* of the V_2O_5 NBs after the first delithiation. (c) XPS spectrum of the Li 1s of the V_2O_5 NBs after the first delithiation.

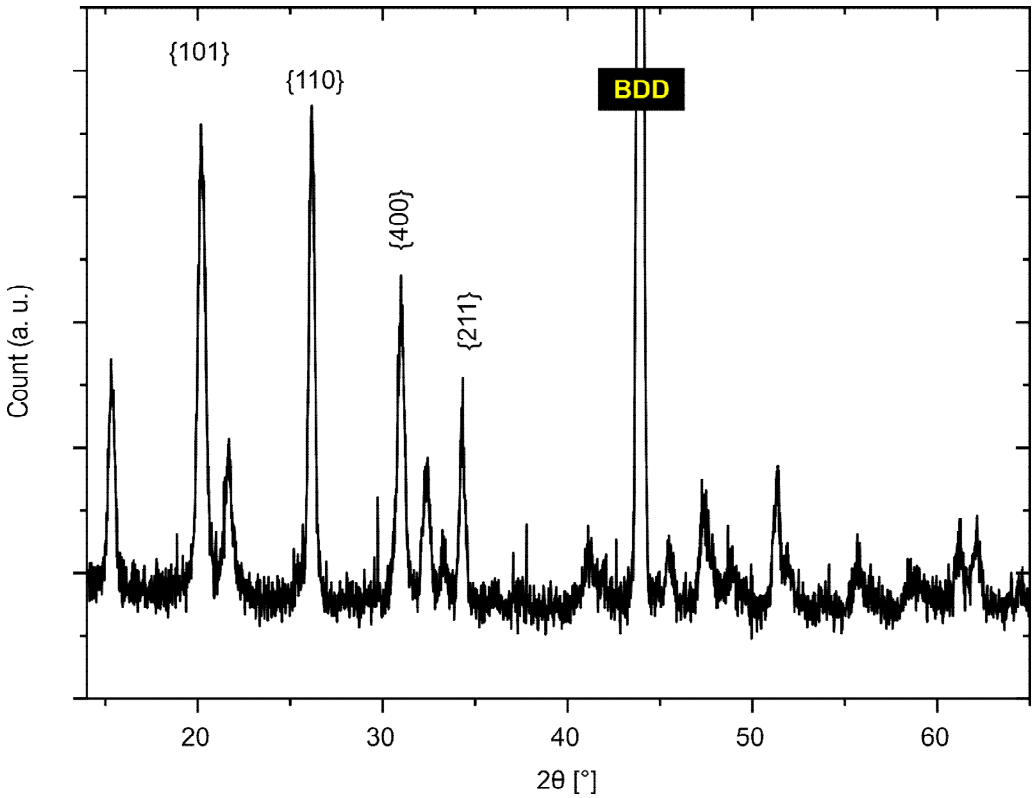

Figure S16: ω-2θ XRD pattern after the first charge (delithiation).

SI13: Electrochemical response during the second discharge and charge cycle and the formation of ordered $Li_3V_2O_5$ structure. Low magnification STEM images of V_2O_5 structures after lithiation and delithiation cycles

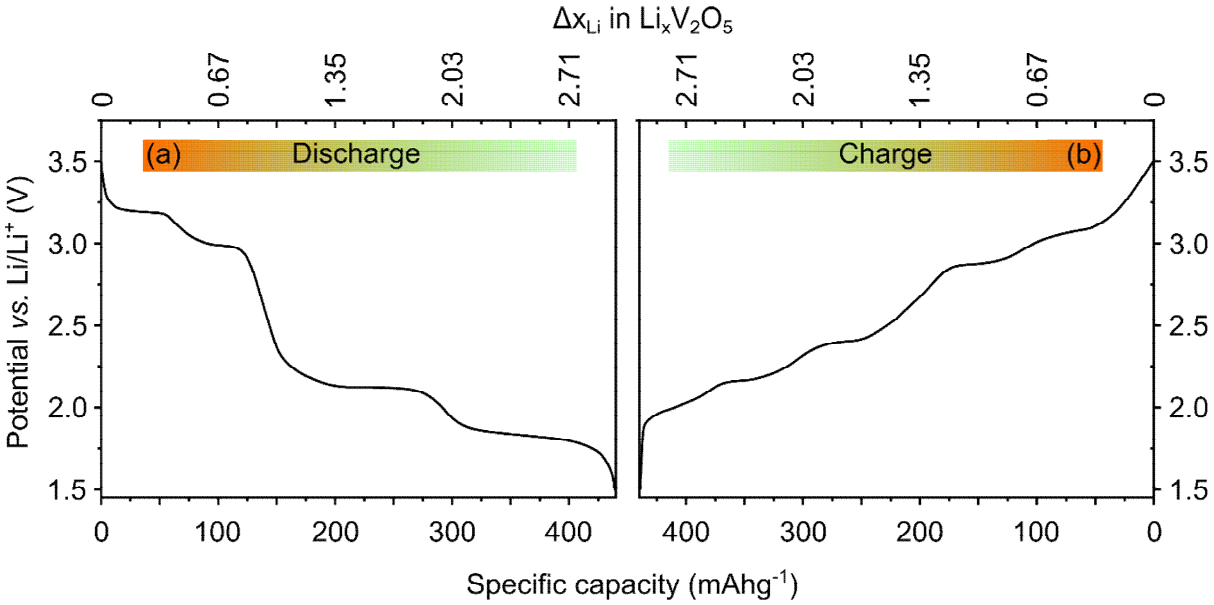

Figure S17: Galvanostatic potential profile. Second discharge (left hand side) – charge (right hand side) of α-V2O5 NB-BDD electrode in 1 M LiCl + 1 M $LiClO_4$ in 1:3 mixture of water and MeCN at C/10 rate.

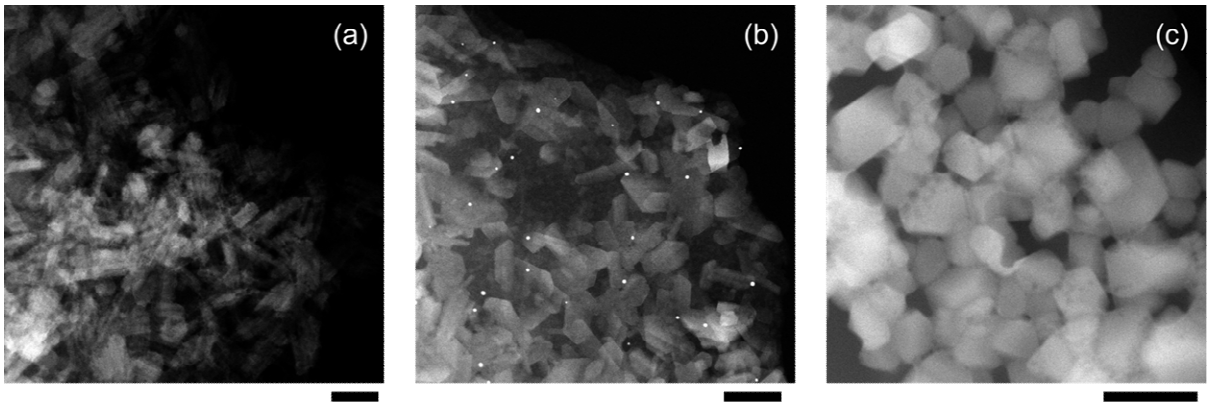

Figure S18: low magnification ADF-STEM images of α-V_2O_5 (a) after first Li intercalation, (b) first Li deintercalation, and (c) second Li intercalation. Scale bar = 100 nm.

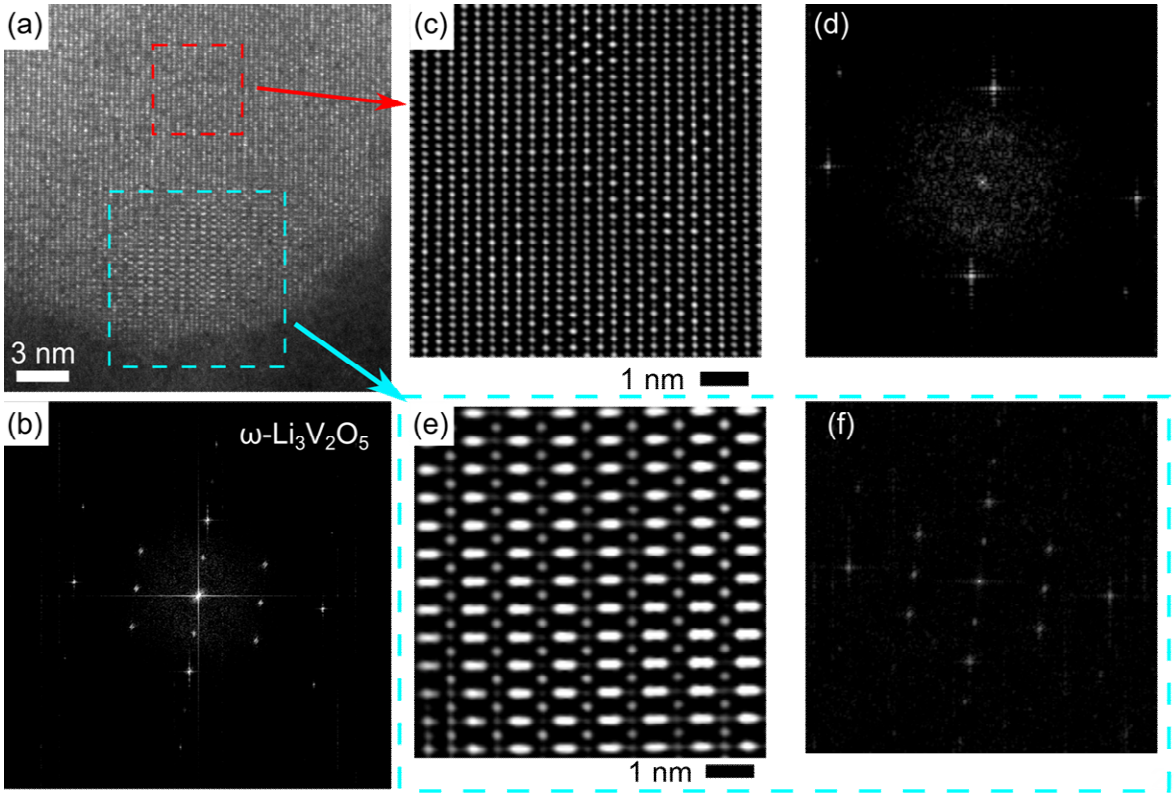

Figure S19: (a) ADF-STEM of a ω-$Li_3V_2O_5$ NB after the second Li intercalation process, and (b) its Fourier transform showing the transformation to structure. (c) Enlarged, Bragg filtered image of the region in (a) that is highlighted by the red square and (d) its Fourier transform. (e) Enlarged, Bragg filtered image of the region in (a) highlighted by the cyan square and (f) its Fourier transform.

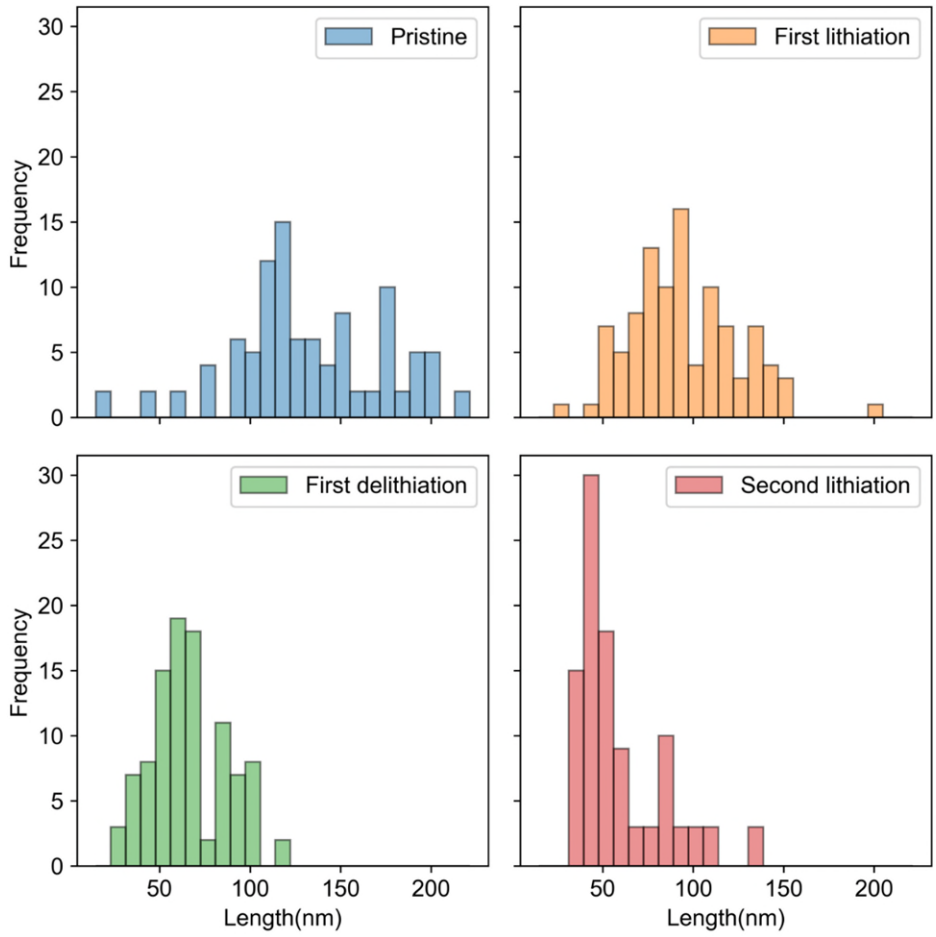

Figure S20: Histogram analysis of changing the length of the V_2O_5 NBs during the lithiation and delithiation process (a) pristine, (b) first lithiation, (c) first delithiation, and (d) second lithiation extracted from low magnification ADF-STEM images.

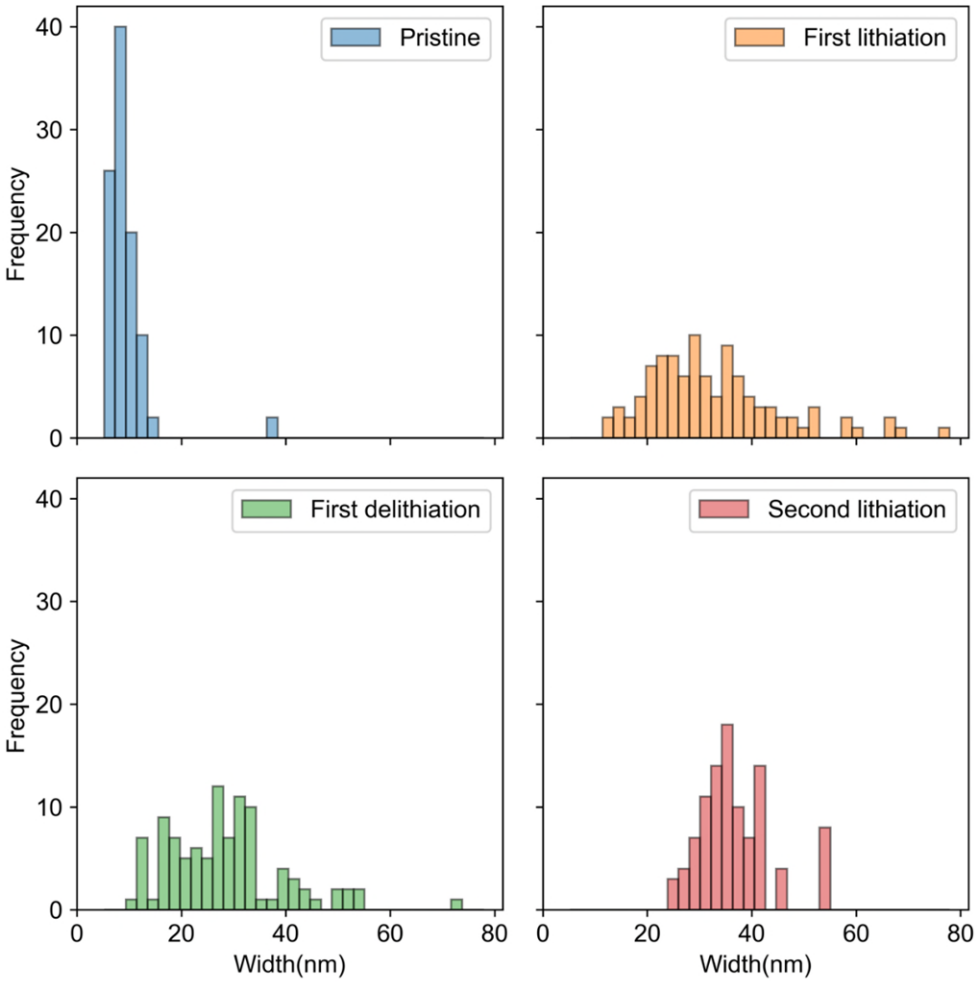

Figure S21: Histogram analysis of changing the width of the V_2O_5 NBs during the lithiation and delithiation process (a) pristine, (b) first lithiation, (c) first delithiation, and (d) second lithiation extracted from low magnification ADF-STEM images.

SI14: References

1. Galy, J., Vanadium pentoxide and vanadium oxide bronzes—structural chemistry of single (S) and double (D) layer MxV2O5 phases. *Journal of solid state chemistry* **1992,** 100, (2), 229-245.
2. Marley, P. M.; Horrocks, G. A.; Pelcher, K. E.; Banerjee, S., Transformers: the changing phases of low-dimensional vanadium oxide bronzes. *Chemical Communications* **2015,** 51, (25), 5181-5198.
3. Ai, R.; Fan, H. J.; Marks, L. D., Phase-transition kinetics in DIET of vanadium pentoxide. 1. Experimental Results. *Surface Science* **1993,** 280, (3), 369-374.
4. Armer, C. F.; Lübke, M.; Reddy, M. V.; Darr, J. A.; Li, X.; Lowe, A., Phase change effect on the structural and electrochemical behaviour of pure and doped vanadium pentoxide as positive electrodes for lithium ion batteries. *Journal of Power Sources* **2017,** 353, 40-50.
5. Armer, C. F.; Lübke, M.; Johnson, I.; McColl, K.; Cora, F.; Yeoh, J. S.; Reddy, M. V.; Darr, J. A.; Li, X.; Lowe, A., Enhanced electrochemical performance of electrospun V2O5 fibres doped with redox-inactive metals. *Journal of Solid State Electrochemistry* **2018,** 22, (12), 3703-3716.

6. Yao, J.; Li, Y.; Massé, R. C.; Uchaker, E.; Cao, G., Revitalized interest in vanadium pentoxide as cathode material for lithium-ion batteries and beyond. *Energy Storage Materials* **2018,** 11, 205-259.